

Recent Gravity Models as a Result of the Lunar Prospector Mission

A. S. Konopliv, S. W. Asmar, E. Carranza, W. L. Sjogren, and D. N. Yuan

Jet Propulsion Laboratory, California Institute of Technology, 4800 Oak Grove Drive, Pasadena, California 91109

E-mail: ask@krait.jpl.nasa.gov

Received June 14, 2000; revised September 27, 2000

The lunar gravity field is determined from the tracking data of previous missions to the Moon with the 1998–1999 Lunar Prospector (LP) mission being the major contributor. LP provided the first measurement of the gravity field in a low polar circular orbit giving complete coverage at high resolution for the entire lunar nearside. However, since there is no direct measurement of the lunar farside from LP or any other mission, gravity details for the farside gravity are greatly limited. Even so, it has become apparent that there are mascons on the farside of the Moon together with the newly identified mascons in the LP data for the lunar nearside. The extended mission low-altitude data (at times less than 10 km above the surface) has gravity information for the nearside to nearly degree and order 180. The 100th-degree lunar gravity models (LP100J and LP100K) extract most of the information from the nominal 100-km altitude. A 165th degree model LP165P attempts to model the extended mission data with some but limited success. This model provides a smooth solution without aliasing when evaluated up to degree 110 allowing for resolution of numerous craters. In addition, a preliminary solution for the lunar Love number is $k_2 = 0.026 \pm 0.003$. © 2001 Academic Press

Key Words: lunar; gravity; spherical harmonics; Doppler.

INTRODUCTION

Lunar Prospector (LP), NASA's third *Discovery* mission and the most recent lunar mission, was launched January 6, 1998 and after a series of maneuvers was placed in a near circular orbit less than two weeks later on January 15 at an altitude of 100 km (see Binder *et al.* (1998) and Binder (1998)). LP remained in this polar ($i = 90^\circ$) 2-h orbit for about one-year for the duration of the nominal mission. This provided global coverage for the gravity experiment every 14 days except for the occultation of the spacecraft whenever it disappeared behind the Moon. On December 19, 1998, the altitude of LP was reduced to an average of 40-km to calibrate the gravity field in preparation for an even lower extended mission. LP began its extended mission on January 29, 1999, when the spacecraft was lowered to an average of 30 km to obtain higher resolution gravity, spectrometer, and magnetic data. At the end of mission on July 31, 1999, the LP spacecraft impacted the lunar surface in an unsuccessful attempt to detect water vapor in the rising dust from impact.

Since there has been no direct observation of the lunar farside gravity by any lunar mission (i.e., it is never visible from the Earth), tracking data from all missions prior to LP have provided important information for the lower degree harmonics (i.e., polar moment of inertia) and large-scale features in the farside gravity. In fact with the LP data only, the farside mascon features discussed in this paper are not visible. The farside gravity information comes from the observed long-term effect on the spacecraft orbit. This farside hole in the gravity data is by far the biggest challenge in processing all the lunar gravity data and obtaining a reasonable gravity solution. The gap is about 33% of the surface since we can track the spacecraft about 20° over the limb. Originally a relay subsatellite was proposed for LP to provide direct measurement of the farside gravity but was canceled in order to reduce cost. However, the Japanese *SELENE* mission in 2003 has a relay subsatellite planned for the direct measurement of the farside gravity.

Study of the gravity field of the Moon began in 1966 with the Russian *Luna 10* mission (Akim 1966) and was followed in August of that same year, by the first U.S. *Lunar Orbiter* (LO-I). By August of 1967, four additional orbiters (LO-II, III, IV, and V) were placed in orbit with various orbital inclinations and eccentricities. Many published their analysis of the gravity field. Using a spherical harmonic expansion of the gravity field, Lorell and Sjogren (1968) produced an 8×4 model, Liu and Laing (1971) a 15×8 model, and Michael and Blackshear (1972) a 13×13 model. Muller and Sjogren (1968), using a new technique of differentiating the Doppler residuals, provided the accelerations along the line-of-sight (LOS) from the tracking station to the spacecraft. This produced a frontside gravity map that displayed large positive gravity anomalies within the large circular maria basins with low topography. This unexpected discovery was opposite of any geophysical model at that time and started the development of new models of the Moon's interior. These features were called mascons (short for "mass concentrations").

In addition to the *Lunar Orbiters*, the *Apollo 15* and *16* missions, in 1971, released two subsatellites with S-band transponders that provided substantial tracking data in retrograde orbital inclinations of 10° and 30° and initial circular altitudes of 100 km. From these data as well as tracking data from the *Apollo Command Service Modules* (CSM), many additional

line-of-sight analyses were performed (e.g., Phillips *et al.* (1972) on the Serenitatis mascon) in addition to surface mass distribution models by Wong *et al.* (1971) and Ananda (1977).

Further spherical harmonic analyses of the lunar gravity were continued into the late 1970s by Ferrari (1977) and Bills and Ferrari (1980), but at most degree and order 16. The resolution of the gravity solutions were limited due to the extensive computational time required. However, with the availability of improved computer power in the 1990s, the Lun60d gravity model of Konopliv *et al.* (1993) extended the resolution to degree and order 60 ($\sim 60^2$ coefficients) using all the available historic data (*Lunar Orbiter I–V*, and *Apollo 15* and *16* subsatellites). Although this first high-resolution model predicts orbit behavior very accurately, it has strong aliasing in the higher degrees (50 to 60), showing a lot of noise in maps of the lunar surface. However, when surface maps are generated only through degree 50 much of the noise is removed, allowing for geophysical interpretation. Subsequent JPL models (e.g., Lun75f) developed prior to *LP* have less noise and maintain the orbit prediction accuracy. More recently, the GLGM-2 model of Lemoine *et al.* (1997) included the *Clementine* tracking data with the same historic *Lunar Orbiter* and *Apollo* data. They showed that the *Clementine* data, acquired in 1994 from an elliptical orbit with a higher periape altitude of 400 km, provided improvement in the low degree ($n = 2, 3$) and sectoral terms (to degree 20) of the gravity field. The *Clementine* laser altimetry data, however, provided the global shape of the Moon for the first time (Smith *et al.* 1997). This topography together with the gravity allowed for substantial improvement in the geophysical modeling of the Moon (Zuber *et al.* 1994).

LP GRAVITY MODELS

The initial models that included the *LP* tracking data were 75th degree (LP75D and LP75G, see Konopliv *et al.* (1998)) and after the nominal mission were followed by 100th degree models (LP100J and LP100K, see Konopliv and Yuan (1999)). These models are available from the Planetary Data System (PDS) Geosciences Node (www.pds.wustl.edu). LP75D was the “30-day” report field and contains tracking data to February 15, 1998. LP75G contains data to April 12, 1998 and was the subject of the last *LP* gravity publication (Konopliv *et al.* 1998). The model highlights included the improvement of the normalized polar moment of inertia by about a factor of 5 (0.3932 ± 0.0002) and the several new mascons at the high-latitude locations on the nearside as well as indications of mascons on the farside of the Moon. Prior to *LP*, all known mascons were on the nearside and associated with large maria-filled impact basins. Several new mascons were found for impact basins with little or no evidence of maria fill, indicating an origin more closely tied to the dynamics of the impact (Neumann *et al.* 1996). With indications of mascons on the farside there is less likely a nearside/farside crustal dichotomy origin for mascon formation. The identification of additional mascon features in the latest higher

degree models (LP100J, etc.) provides additional support for this interpretation.

The LP100J model includes all the *LP* Doppler and range data through February 8, 1999, that is, all the nominal mission data in the 100-km orbit, all the 40-km average altitude data of about 40 days, and the first 10 days of the 30-km average altitude orbit. A similar follow-on model (LP100K) added the rest of the extended mission data and, thus, contained all the tracking data from the *LP* mission. The LP100K model is only a slight improvement over LP100J with the surface features being nearly identical. All the *LP* models also include all the available data from the previous missions of *Lunar Orbiter I–V*, the *Apollo 15* and *16* subsatellites, and *Clementine* as described by Konopliv *et al.* (1993) and Lemoine *et al.* (1997). The LP100J and LP100K models probably provide the best orbit determination accuracy versus computational time required to determine the orbits and would be the models suggested for the initial operational use for *SELENE* or other future missions. LP165P provides the best accuracy but may take excessive computer time because of the high degree and order. Typical orbit uncertainties for the *LP* nominal mission were 0.5 m in the radial direction (altitude) and 5 m in the other two directions (along the velocity vector and normal to the orbit plane); see Carranza *et al.* (1999) regarding orbit overlap analysis using LP100J. Because of the farside hole in the gravity and the associated large uncertainty, the gravity field will have to be tuned for orbits that are not an exact repeat of the *LP* orbits. For example, without fine-tuning of the gravity field using the expected *SELENE* data, the orbit error would be about 20 m radially and on the order of 1 km in the alongtrack direction when using LP100J, LP100K, or LP165P. Fine-tuning of the gravity field by including the *SELENE* tracking in the gravity solution would reduce the error to the *LP* levels. However, the *LP* models should accurately predict the altitude behavior of any circular orbit for inclinations greater than 80° (to several hundred meters for month-long predictions).

The 100th degree models extract most of the gravity information from the nominal 100-km altitude mission with very little signature left in the remaining Doppler residuals. However, with the extended mission, *LP* at times reached to within 10 km of the actual surface especially over the south pole mountains and farside highlands. In general, the extended mission contains gravity information to roughly degree 180. An attempt has been made to model the gravity field to degrees higher than 100 but not quite to 180. Using a method similar to the determination of the 180th degree model for Venus (Konopliv *et al.* 1999), a 165th degree model (LP165P) was estimated in multiple steps. This solution is complete to degree 122 ($\sim 15,000$ coefficients) and then using the solution to degree 122 as the a priori, the gravity is estimated in segments to degree 145 ($\sim 6,000$ coefficients) and then 165 ($\sim 6,000$ coefficients) where each time the new solution is used as the a priori for the next. However, this process has not been as successful as in the Venus case. There is strong aliasing at the end and beginning of the cutoff degrees 122 and 145 and it is most likely due to the lack of global coverage from the farside

hole. As a result of this data gap, the coefficients are strongly correlated and estimating the field in sections becomes difficult. The field represented to about degree 110 is very clean with very little data noise, but for instance, at degree 140, it shows noticeable noise in the gravity maps at the lunar surface. As for the farside, all fields show considerable noise, although there is still significant gravity information. Still LP165P provides the best fit to the data as shown by the Doppler residuals, provides much better orbit accuracy versus LP100J or LP100K for the extended mission (about 2 m radially and 20 m in the other directions), and provides clean spectral information without aliasing to degree 110 (versus degree 90 for the 100th degree models). It is the first cut at the higher frequencies to degree 165 that is useful for nearside studies. Even so, future models that solve for all coefficients in a single step will be much better. Although at this time, the high-degree models are difficult to evaluate because of the lack of global high-resolution topography. The best global model currently available is the *Clementine* lidar model GLTM2 to degree 90 (Smith *et al.* 1997).

The high-frequency information in the LP data is also available for study with the LOS data that has been delivered to the PDS Geosciences Node as above and includes all the Doppler data from the nominal and extended mission. In similar form to the *Magellan* gravity LOS investigations (e.g., Barriot *et al.* (1998) and McKenzie and Nimmo (1997), the Doppler residuals are with respect to a higher resolution gravity model (in this case, LP100J) and thus contain the gravity signature beyond the modeled degree.

GRAVITY DATA

All the lunar missions used in determining the gravity field (*LO*, *Apollo*, *Clementine*, *LP*) were tracked at the S-band frequency (2.2 Ghz), and all but *Apollo* were tracked with the NASA/JPL Deep Space Network (DSN) complexes in California, Spain, and Australia using 26-m stations and, for *LP* and *Clementine*, with the 34-m stations as well. The *Apollo* subsatellites were tracked with 14 stations of the now non-existent Manned Space Flight Network (MSFN). The uplink S-band signal to the spacecraft (2093 MHz for *LP*) was coherently multiplied by 240/221 by the spacecraft transponder and retransmitted to either the same Earth station (2-way data) or to a different receiving station (3-way). The 3-way Doppler data for *LO* and *Apollo* were processed. The *LP* spacecraft did not have a data recorder and so required near continuous tracking to downlink the instrument data (a plus for the gravity experiment), so only 2-way Doppler plus range data were processed.

In terms of data quality, the older *LO* data contained many uncoupled maneuvers to point the spacecraft for picture taking. These turns not only introduced antenna motion into the Doppler data but dynamically broke the gravity information in the data arc. The *LO-V* data set is exceptionally noisy from a possible hardware problem. Even so, the entire *LO* data set is important for the determination of farside gravity features. The first three

Lunar Orbiters were near equatorial with inclinations between 10° and 20° . *LO-IV* was near polar ($i = 85^\circ$) but was very eccentric and provided little gravity information. *LO-V* also was near polar ($i = 85^\circ$) but less eccentric with periape at the equator with an altitude of 100 km. When over the poles, the *LO-V* altitude was 600 km. For all but the LP165P solution, the *LO* data set is weighted with an accuracy of about 1.0 mm/s except for parts of the *LO-V* data, which were weighted near 10 mm/s. In general, the weight of the data is near the RMS of the Doppler residuals. The LP165P solution slightly deweights the historic *LO* and *Apollo* data by a factor of 1.8.

The *Apollo 15* and *16* subsatellites were simple spin-stabilized spacecraft released from the *Apollo CSMs*. They performed no propulsive maneuvers and so are ideal for gravity study. The *Apollo 16* subsatellite was released in a 10° inclined circular orbit (a retrograde $i = 170^\circ$ inclination) with a 100-km altitude and impacted the Moon 35 days later strictly due to the influence of the gravity field. The lifetime or long-term behavior of a spacecraft in a low near-circular orbit is only dependent on the zonal coefficients of the gravity field (e.g., Konopliv *et al.* (1993)). For a given semi-major axis, the maximum lifetime is a function of the inclination of the orbit. The zonal effect is so strong at a 10° inclination, that any orbiter with a 10° inclination and average 100-km altitude would likewise impact. In contrast, the *Apollo 15* subsatellite was released in a circular retrograde $i = 151^\circ$ inclination (or 29° relative to the equator) at an altitude of 100 km and lasted for several years. At times it was sparsely tracked (one hour or one orbit per day) and so the gravity information is very limited in this data. In fact, multiple day arcs are difficult to converge with this limited tracking. There were several dedicated tracking times of one or two weeks with tracking every third orbit that provided a lot of farside information. There is no problem of orbit convergence with this much tracking. Except for LP165P, the typical data weight is again near 1.0 mm/s.

The *Clementine* mission provided tracking data for the gravity field from February 19 to May 4, 1994, where for one month periape was located at 30°S and for the next month at 30°N (both with a 415 periape altitude). About two-thirds of the tracking of *Clementine* was from the DSN with 10-s compression times and an RMS data noise near 0.3 mm/s. Although for this gravity investigation, the data were compressed to 60 s outside a 1-h interval around periape. The remaining tracking was from the Pomonkey station of the Naval Research Center. The data noise from this station was much higher at near 3 mm/s (Lemoine *et al.* 1997). Because of tracking file conversion problems, the Pomonkey data were not included in the JPL gravity solutions but this has a very small effect. Although the Doppler RMS was somewhat smaller than *LO*, the *Clementine* data were weighted also near 1.0 mm/s for all solutions. Lemoine *et al.* (1997) and Konopliv *et al.* (1993) give good overviews of the historic *LO*, *Apollo*, and *Clementine* data.

The behavior of the *Apollo 16* subsatellite is a dramatic display of the strong influence of the gravity field on the orbit. The

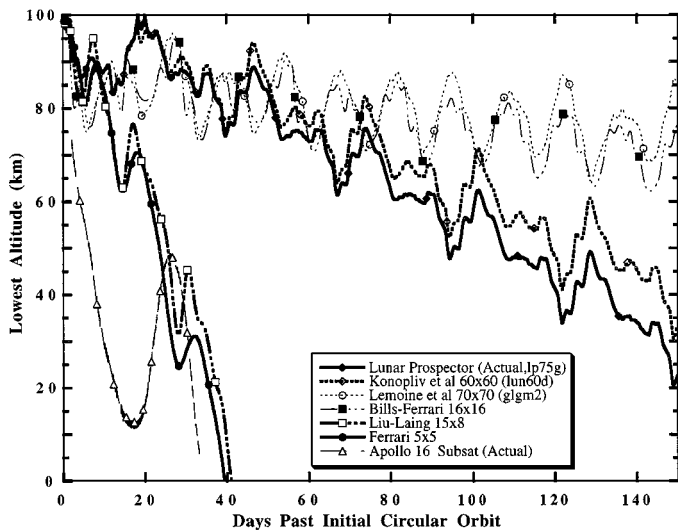


FIG. 1. Predicted orbit behavior for *LP*. Each curve displays how the periapee altitude of the *LP* orbit changes with time for a given gravity field as determined by numerical integration of the orbit. Except for the last curve, the initial conditions are given by the *LP* orbit after it was circularized on January 15, 1998. The last curve shows the actual periapee decline for *Apollo 16* with its 10° inclination.

challenge for *LP* was determining the long-term trend of the spacecraft altitude since no prior spacecraft orbited the Moon in a low-altitude circular polar orbit. If the altitude dropped like *Apollo 16*, then the *LP* mapping orbit would be very different and the mission would last at most 6 months with no extended mission because all the fuel would be used to maintain a safe altitude. There was a wide range of possible behaviors predicted by propagating different gravity fields. Figure 1 shows the actual behavior observed for *LP* once it was inserted into a circular orbit on January 15, 1998, together with the predictions from five gravity fields determined prior to *LP* (Lun60d of Konopliv *et al.* (1993), and GLGM-2 of Lemoine *et al.* (1997), Bills and Ferrari (1980), Liu and Laing (1971), and Ferrari *et al.* (1980)). The predictions from the *LP*-based models (*LP75G*, etc.) match the actual observed altitude and so correctly incorporate the long-term trend of *LP*. The actual *LP* altitude ends after 60 days when a maneuver was performed to raise the altitude. In addition, the altitude drop for the *Apollo 16* subsatellite is shown as an example of possible behavior even though it has a different orbit inclination. The Lun60d model was chosen to design the mission and it turned out to provide the best prediction of any available model. The differences of being out of phase after 20 days in the model predictions of the more recent models (Lun60d and GLGM-2) have been traced to differences in coefficients as low as degree 10. However, when looking at the RMS discrepancy beyond the associated uncertainties of the gravity fields, the wide range of predictions is really a consequence of the lack of farside gravity data.

With the altitude behavior in the initial *LP* orbit shown to be reasonable, the altitude could easily be maintained between 80

and 120 km for uniform collection of the spectrometer data. A maneuver was required every 2 months to adjust the orbit. This resulted in a repeat pattern for the spacecraft altitude with a period of 56 days very similar to the first 56 days of Fig. 1. The extended mission data set was broken into two equal phases of three months each. The first three months of the 30-km average altitude orbit as well as the 40-km altitude orbit had periapee on the nearside of the Moon and the last three months of the extended mission had periapee on the farside of the Moon. Together, the spacecraft minimum altitude over any given region of the Moon was roughly 20 km, but of course no direct tracking for the farside. For the extended mission, as for the nominal mission, the mapping involved repeat orbits. A maneuver was performed every 28 days to initiate the repeat orbit behavior with a separate repeat orbit for each three-month interval. For each 28-day repeat pattern, the periapee altitude varied from 12 to 29 km above the mean surface, and the latitude of periapee greatly varied over all latitudes.

Overall, the Doppler data accuracy for *LP* is near 0.3 mm/s using a 10-s sample time. The DSN beam waveguide 34-m stations (e.g., DSS 24) provided the best data accuracy of 0.2 mm/s and the 26-m station data noise varied between 0.3 and 1.0 mm/s. So, for the nominal mission the *LP* data weight was 1.0 mm/s for all but the *LP165P* solution, which used a slightly tighter weight of 0.8 mm/s. For the extended mission, however, there was a significant increase in the data noise for near the polar regions. Lowering the spacecraft's altitude in the extended mission brought the antenna close to the lunar surface and, thus, caused the transmitted radio signal to be scattered by the surface. The ground antennas received the radio signal in the direct path as well as additional background noise reflected from the surface. The tracking receivers produced noisier Doppler data as the signal-to-noise ratio decreased. The data were less noisy away from the poles and subsequent occultations by the lunar polar surface, as the antenna was directed to Earth in a line-of-sight away from the surface. This problem was better understood after utilizing another type of receiver that is used for occultations and other radio science experiments, which is an open-loop receiver. A downconverted preselected portion of the spectrum was recorded in a wide bandwidth and digitized for post-processing, as opposed to real-time processing by the tracking receiver. The analysis revealed the scattering effect near the carrier signal. A scattering effect was also seen in the Doppler from the nominal mission but was much less pronounced because of the higher altitude. Anyone processing the *LP* extended mission data (including LOS analysis) should be aware of this problem as well as any future missions planning low orbits. For the purpose of the gravity solutions, any data with excessive noise ($> \sim 2\text{--}3$ mm/s) were removed.

In addition, with the much lower altitude for the extended mission, the mismodeled farside gravity had a much stronger effect on the RMS fit of the data arcs. With two-day data arcs it was impossible to adjust the gravity field to fit to the data noise. The data arcs with periapee on the nearside fit better and a data weight of 2.0–3.0 mm/s was used. The data arcs with periapee

TABLE I
Summary of Tracking Data in the Gravity Solutions

Mission	Gravity fields	Number of arcs	Typical arc length (days)	Number of observations
<i>Lunar Orbiter I</i>	All	58	1	37,651
<i>Lunar Orbiter II</i>	All	82	1	69,827
<i>Lunar Orbiter III</i>	All	48	1	56,472
<i>Lunar Orbiter IV</i>	All	5	3	9,309
<i>Lunar Orbiter V</i>	All	41	1	39,752
<i>Apollo 15</i> subsatellite	All	21	3	45,438
<i>Apollo 16</i> subsatellite	All	7	4	25,475
<i>Clementine</i>	All	29	3	97,055
<i>LP</i> 100-km nominal mission (subset) Jan. 15, 1998–Feb. 15, 1998	LP75D	23	2	250,520
<i>LP</i> 100-km nominal mission (subset) Jan. 15, 1998–April 12, 1998	LP75G	36	2	604,997
<i>LP</i> 100-km nominal mission (all) Jan. 15, 1998–Dec. 19, 1998	LP100J LP100K LP165P	176	2	2,282,094
<i>LP</i> 40- and 30-km extended mission (subset) Dec. 19, 1998–Feb. 8, 1998	LP100J	24	2	306,909
<i>LP</i> 40- and 30-km extended mission (all) Dec. 19, 1998–July 31, 1999	LP100K LP165P	111	2	1,366,759

on the farside (the last three months of the mission) had data weights near 4.0–6.0 mm/s. The *LP* range data noise, however, is consistent for the entire *LP* mission with an RMS noise of about 0.5 m for the 1000-plus range points collected every day of the mission but with a 2-m data weight used in the gravity solution. However, the range data do not strongly influence the gravity solution. Since *LP* was in a circular polar orbit, the groundtracks converge near the pole and the observations become more dense. For this reason, the *LP* observation weighted sigma is adjusted for latitude ϕ ($\sigma_{\text{new}} = \sigma_{\text{old}} * \cos^{-1/2} \phi$) with a maximum deweighting factor of 50 used for points within a degree of the pole. The inclination of *LP* had long-term variations within about 1° of the exactly polar $i = 90.0^\circ$.

Table I lists the missions included in the gravity solutions along with the number of observations (two- and three-way Doppler plus range for *LP*) and typical arc length. For each given arc, the spacecraft position and velocity are estimated with the spacecraft trajectory being continuous over that time interval. For *LP*, the data arcs are typically 2 days long or 24 orbits. The lengths of the arcs were chosen to maximize the amount of gravity information included in the solution while minimizing the negative effects of unmodeled nonconservative forces on the spacecraft that increase with longer arc lengths. The lack of farside data makes it more difficult to choose the appropriate arc

length since, for example, irregular solar pressure solutions may be due to errors in the farside gravity. Arcs could be confidently longer if farside gravity were observed.

LP SPACECRAFT

The *LP* spacecraft is a simple spin-stabilized cylindrical spacecraft with a height of 1.3 m and a diameter of 1.4 m. The outside of the drum is covered with solar arrays and three equally spaced 2.5-m masts are attached. These booms are normal to the spin axis and hold the spectrometer and magnetic instruments (see lunar.arc.nasa.gov or wwwpds.wustl.edu for more information on the spacecraft and *LP* mission). The dry mass of the spacecraft was 158 kg. After lunar orbit insertion 33 kg of propellant remained, of which 14 kg was used throughout the nominal mission. *LP* utilized an S-band (2.2-GHz) communications system with the same model Loral-Conic transponder as the *Clementine* mission. The spacecraft had two antennas both placed as near to the spin axis or cylindrical axis of symmetry as possible. The omni antenna was always used for the up-link signal and sometimes for the down-link. However, the medium gain antenna was mostly used for transmitting the signal back to Earth. The spin axis was pointed to within 10° of the ecliptic north for the first nine months of the mission and to within 10° of the ecliptic south for the remainder of the mission. The spin of the *LP* was maintained to within 0.1 rpm of the nominal 12 rpm or 5-s period.

The spacecraft spin introduces two separate effects into the Doppler data. First, the spin introduces a bias in the Doppler due to the spacecraft antenna pattern rotating with respect to the Earth station. For the case where the omni antenna is used for both the up-link and down-link, a bias of $(1 + 240/221) \times S$ Hz is the result where S is the spin rate of the spacecraft in revs/s (0.2 for *LP*). The bias is thus 0.417 Hz or 27.3 mm/s (1 mm/s = 0.0153 Hz at S-band). For the medium gain antenna, the polarization changes and the bias is $(1 - 240/221) \times S$ Hz, which for *LP* is -0.0172 Hz or -1.12 mm/s. In addition to the bias and a completely different effect, a sinusoidal signature appears in the high-rate (1-s) Doppler data due to an offset of the antenna phase center from the spacecraft spin axis. Although the phase center was placed as close to the spin axis as possible, a small offset still causes a large signature in the Doppler. When the omni antenna is used for both the up-link and down-link signal, the result is a signature with a 5-s period and 8.15-mm/s amplitude. This indicates a 6.4-mm offset of the omni antenna phase center from the spin axis. The amplitude reduces to 4.5 mm/s when the medium gain antenna is used for the down-link. Since the Doppler data are essentially differenced range measurements from the end points of the observable integration time, the sinusoidal signature can mostly be removed by using a multiple of 5 s for the Doppler sample time. For the gravity models described in this work, a sample time of 10 s is used. After 10 s, the antenna phase center has returned to nearly the same location and this results in a very small remaining sinusoidal

signature of less than 0.1 mm/s. This small signature is the result of the spacecraft spin not being exactly 5 s.

The spacecraft spin also had to be characterized for the LP open-loop recordings of the carrier signal for the purpose of timing the occultation events. The amplitude modulation showed that the spin period changed over the course of the mission but varied by less than 1% over any one orbit.

GRAVITY MODELING

All the lunar mission observations were processed using JPL's Orbit Determination Program (ODP) (see Moyer (1971)); the software set used at JPL for navigation of all planetary spacecraft. The ODP was modified for use on the Caltech/JPL HP Exemplar SPP2000 supercomputer and it estimates the spacecraft state and other parameters using a square root information weighted least-squares filter (see Lawson and Hanson (1995), Bierman (1977)) in the coordinate system defined by the Earth's mean equator at the epoch of J2000. The parameters that are estimated consist of arc-dependent variables (spacecraft state, etc.) that are determined separately for each data arc and global variables (harmonic coefficients, etc.) that are common to all data arcs. The global parameters are determined by merging only the global parameter portion of the square root information arrays from all the arcs of *LO*, *Apollo*, *Clementine*, and *LP*, but is equivalent to solving for the global parameters plus arc-dependent parameters of all arcs. This technique is described by Kaula (1966) using partitioned normal matrices and was first used to analyze Earth orbiter data, and for the type of filter used in this work (square root information), the method is outlined by Ellis (1980).

Initially, we converge the data arcs by estimating only the local variables using the nominal values for the global variables. For each data arc the local variables estimated are the spacecraft position and velocity, three solar pressure coefficients, velocity increments for the photographic maneuvers of *LO*, biases for each three-way Doppler data pass due to the clock offsets between stations, range biases for each station pass (*LP* only), and also for *LP* a Doppler bias every arc for any small corrections to the spin-induced bias mentioned above. The solar pressure model is a simple bus model that estimates the solar pressure force along the Sun–spacecraft direction and the two orthogonal directions toward the ecliptic pole and in the ecliptic plane. This model will absorb any possible spacecraft outgassing or thermal radiation. In addition to the estimated parameters, there are many different models involved in the estimation process including, for example, accurate Earth station position modeling (to the 2–3 cm level), ionospheric and tropospheric corrections to the Doppler and range data that are based on in situ GPS and weather measurements, point mass accelerations due to the Sun and planets, relativistic time delay corrections on the observable, Earth's oblateness on the spacecraft, and the indirect oblateness or the acceleration of the Moon due to the Earth–Moon oblateness interaction.

In general, the *LP* spacecraft is very clean with no momentum wheel desaturations and no atmospheric drag to estimate. The solar pressure force is simple because of the cylindrical bus and limited components (no solar panels or large antennas). Although outgassing of some sort is evident in the solar pressure solution at the beginning of the mission and decays to negligible values after the first 30 days of the mission, *LP* is a good spacecraft to study the long-term effects of the gravity field. Of course the major limiting factor in its use is the lack of direct farside gravity observation. If the farside is mapped by a future mission, the *LP* data should provide excellent information on the k_2 Love number for example. A maneuver was performed to adjust the *LP* spacecraft altitude about every 56 days for the nominal mission and every 28 days for the extended mission. None of these large maneuvers were included in a data arc since data arcs were chosen to begin and end at maneuver times. Typically every two weeks, an additional small maneuver was performed to adjust the spin rate or spin pole direction. Data arc start and stop times were also chosen to occur at these maneuver times to limit nongravitational mismodeling.

The gravitational potential of the Moon is modeled by a spherical harmonic expansion with normalized coefficients (\bar{C}_{nm} , \bar{S}_{nm}) and is given by

$$U = \frac{GM}{r} + \frac{GM}{r} \sum_{n=2}^{\infty} \sum_{m=0}^n \left(\frac{a_e}{r}\right)^n \bar{P}_{nm}(\sin \phi) \times [\bar{C}_{nm} \cos m\lambda + \bar{S}_{nm} \sin m\lambda],$$

where n is the degree and m is the order, \bar{P}_{nm} are the fully normalized associated Legendre polynomials, a_e is the reference radius of the Moon (1738.0 km for our models), ϕ is the latitude, and λ is the longitude. The normalized coefficients are related to the unnormalized by (see Kaula (1966))

$$(\bar{C}_{nm}; \bar{S}_{nm}) = \left[\frac{(n+m)!}{(2-\delta_{0m})(2n+1)(n-m)!} \right]^{1/2} (C_{nm}; S_{nm}),$$

where δ_{0m} is the Kronecker delta function. The harmonic coefficients of degree one are fixed to 0 since the origin of the coordinate system is chosen to be the center of mass of the body.

The lunar gravity field was developed using the lunar orientation specified by JPL planetary ephemeris DE403. On the ephemeris, the orientation of the Moon with respect to the Earth mean equator of J2000 (EME2000) is given by three Euler angles (Newhall and Williams 1997): (1) the rotation by angle φ about the Z axis from the vernal equinox or X axis of EME2000 to the intersection of the ascending node of the lunar equator, (2) the tilt up about the X axis by θ to match the lunar equator, and (3) the rotation by ψ along the lunar equator to the lunar prime meridian. These three angles describe the lunar librations to a very high accuracy (2–3 cm accuracy for the lunar laser ranging, Dickey *et al.* (1994)) and were determined from numerically integrating the lunar orientation together with the planetary

positions. These three angles give a lunar body-fixed coordinate system with axes aligned with the lunar principal axes.

All the results of the lunar gravity fields presented here use the body-fixed lunar orientation of DE403. If, however, one wishes to use the lunar gravity field with the IAU lunar pole and prime meridian, some corrections must be made. The IAU orientation, either IAU-1991 (Davies *et al.* 1992) or IAU-1994 (Davies *et al.* 1996), is also a lunar body-fixed orientation with some lunar librations included but with the body-fixed axes specified by the mean pole of the Moon. These axes are offset from the principal axes of DE403 by rotations using three small angles and amounts to about 700 m at the lunar surface for two of the angles. The conversion from mean (M) axes of the IAU to the principal axes (P) is given by Williams *et al.* (1996) for DE245. The angles for DE403 change slightly and are

$$P = R_z(63.8986'')R_y(79.0768'')R_x(0.1462'')M.$$

These rotations can also be included in the right ascension ($\alpha = \varphi - 90^\circ$), declination ($\delta = 90^\circ - \theta$), and prime meridian ($W = \psi$) series of the IAU by adding more terms to the series. To convert the IAU series (either 1991 or 1994) to the principal axes used by DE403, add $0.0553 \cos W_p + 0.0034 \cos(W_p + \Omega)$ to α , add $0.0220 \sin W_p + 0.0007 \sin(W_p + \Omega)$ to δ , and add $0.01775 - 0.0507 \cos W_p - 0.0034 \cos(W_p + \Omega)$ to W , where $\Omega = E1$ of the IAU series and W_p is the polynomial part of W (J. G. Williams 1994, personal communication). These terms come from spherical trigonometry relations for the three small rotations above. With the IAU series converted to the principal axes, the remaining differences between the DE403 coordinate frame and the IAU are due to truncation of the libration terms in the IAU series. Figures 2 and 3 show the magnitudes of the position differences in the body-fixed axes on the lunar surface of the corrected IAU-1991 and IAU-1994 coordinates, respectively, with the DE403 axes. The results of using the IAU-1991

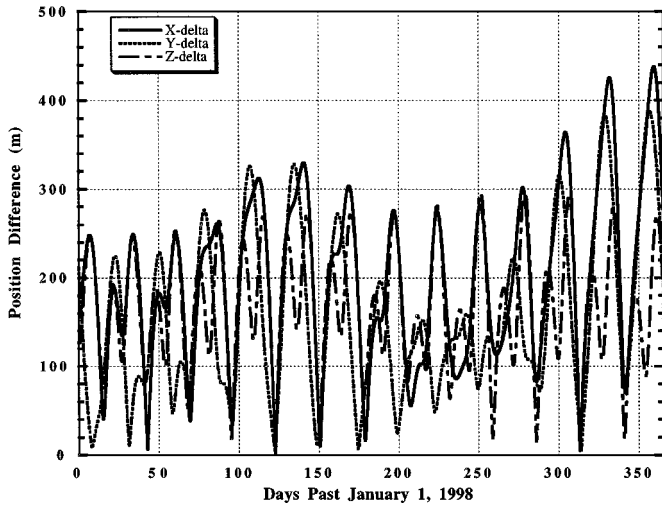


FIG. 2. Differences of the lunar axes on the lunar surface from the DE403 integrated lunar librations and the 1991 IAU mean pole.

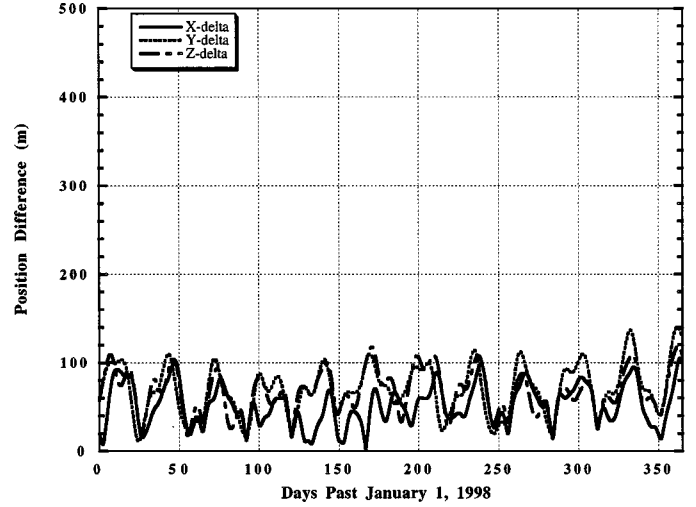


FIG. 3. Differences of the lunar axes on the lunar surface from the DE403 integrated lunar librations and the 1994 IAU mean pole.

axes amount to errors in lunar orientation of 440 m during the *LP* nominal mission, whereas the maximum errors from using IAU-1994 are 140 m.

GRAVITY RESULTS

Once all the observables are processed into one information array, the gravity field needs to be constrained because of the large farside gap in the gravity data. If there is no constraint the coefficients take on unrealistically large values. Figure 4 shows the lunar gravity solution with the above-mentioned data for an unconstrained 50th degree solution (LP50PNOAP, i.e., no a priori). The large fluctuations in the gravity field (purple/black region) clearly show the gap where there is no direct farside observation of the gravity field. Where there are no large fluctuations, the gravity field is well determined, and so this figure is useful to show which features can be studied in detail with the *LP* gravity fields.

The typical constraint method is to bias the coefficients toward 0 based upon a power law versus the degree of the coefficient. The previous lunar gravity solutions (Lemoine *et al.* 1997; Konopliv *et al.* 1993, 1998) have used this method with an inverse square of the degree n (power law $\sim 1/n^2$). Recent Mars gravity models have used the power constraint for only the high-frequency terms such as $n > 50$ (Smith *et al.* 1999, Yuan *et al.* 2000). Another constraint method is to constrain the solution spatially instead of a spectral constraint. This method proved useful for the high-resolution model of Venus (Konopliv *et al.* 1999) where there is substantial regional variation in data resolution and also for a pre-MGS gravity model (Konopliv and Sjogren 1995) to correctly specify the amplitudes of the Tharsis volcanoes. The use of this technique, however, has not been as successful for the lunar gravity models. The farside gap is too large to result in a reasonable power spectrum with a spatial constraint. When the spatial constraint is applied, there is too much

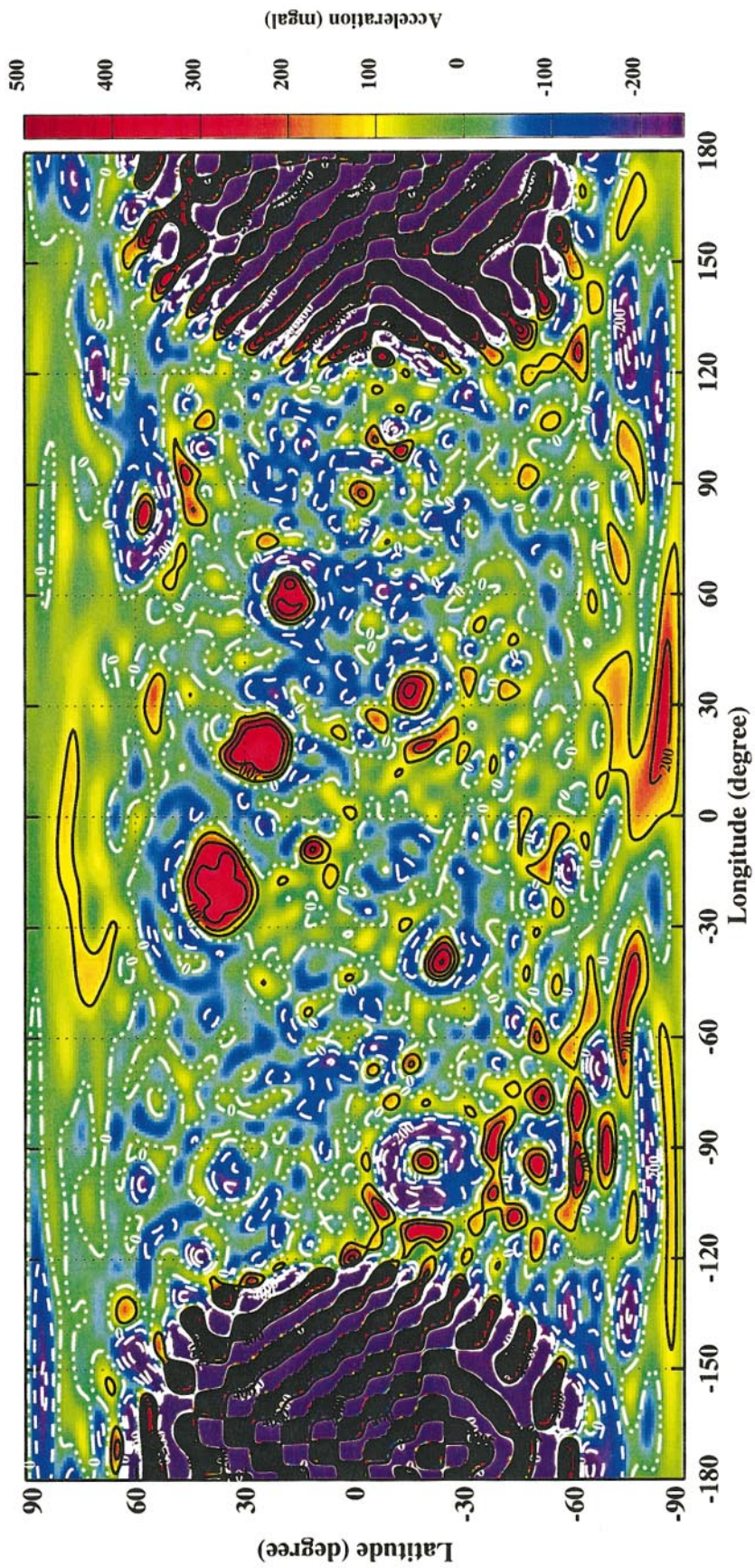


FIG. 4. Unconstrained 50th degree and order lunar gravity field (LP50PNOAP for no a priori) accelerations at the lunar surface. Large oscillations on the lunar farside indicate where there is no direct observation of the gravity field.

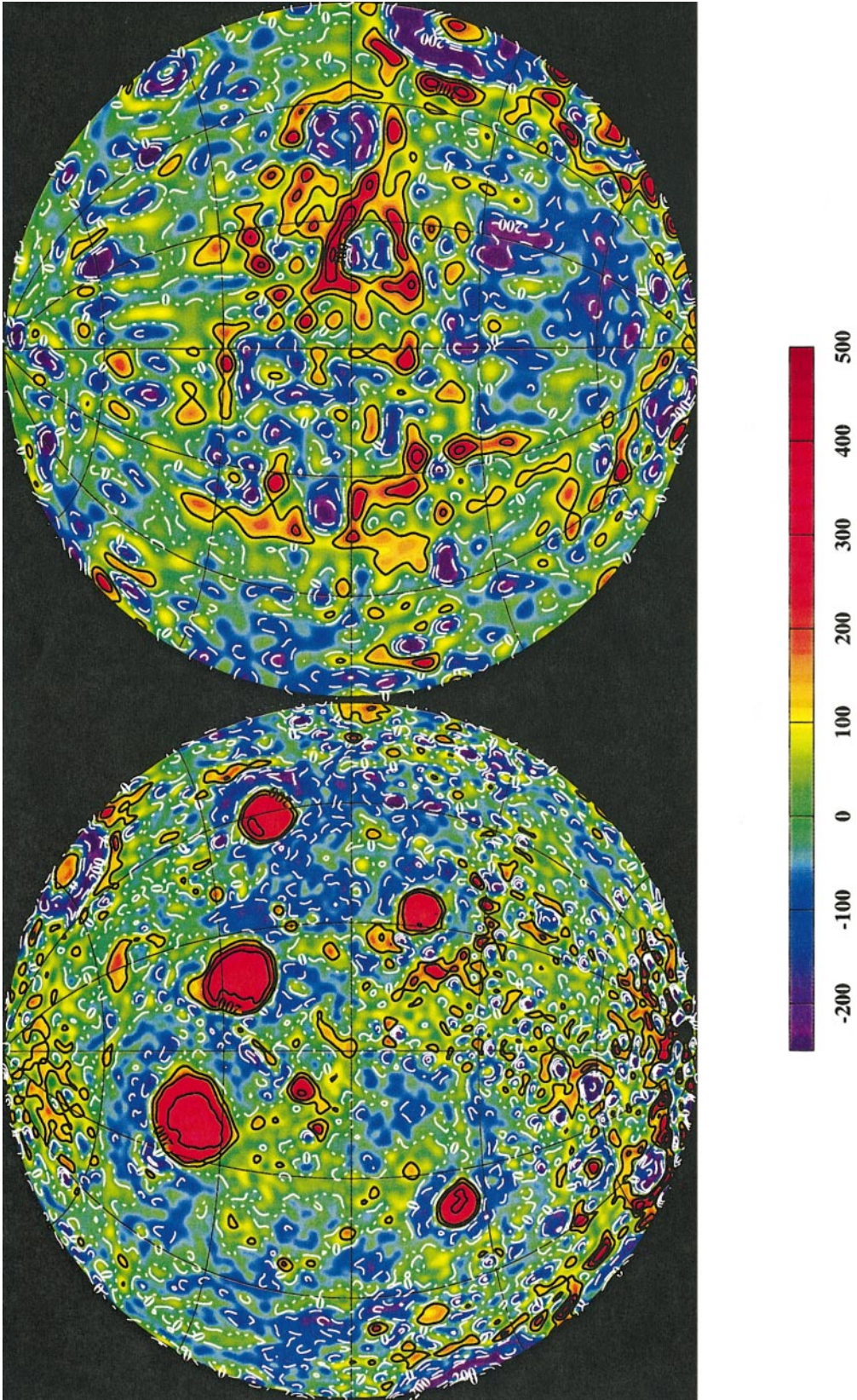


FIG. 8. Vertical acceleration at the lunar surface for the LP165P gravity field. Accelerations are the radial component at the lunar reference sphere with radius 1738.0 km. The nearside (on the left) includes coefficients to degree and order 110. The farside (on the right) displays terms to only degree and order 60 in order to limit noise in the image. Both have the J_2 coefficient (or flattening) removed. Units are milligals with contour lines every 100 milligals.

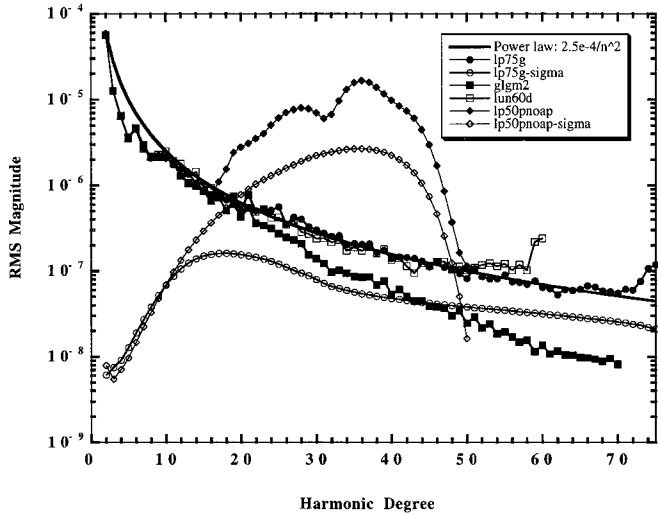


FIG. 5. RMS magnitude spectra for the lower degree and order lunar gravity solutions. Included is the unconstrained 50th degree and order solution displayed in Fig. 4.

power in the higher frequencies. The constraint strongly affects the power in the RMS magnitude spectrum for degrees greater than about 15. So, again, a spectral constraint is used for these *LP* gravity models (for LP100J, LP100K, LP165P use $3.6/n^2$, which is slightly greater than the actual observed spectrum).

Figure 5 shows the RMS magnitude spectra for the higher resolution gravity models prior to *LP* (Lun60d of Konopliv *et al.* (1993), GLGM2 of Lemoine *et al.* (1997)), one of the first *LP* gravity models LP75G of Konopliv *et al.* (1998), and a 50th degree lunar gravity model with the same data set as LP165P but with no gravity constraint (LP50PNOAP for no a priori). The Lun60d model has very near the same power as the *LP* models except for the aliasing in the higher degrees (50 to 60) where there is too much power (and noise as discussed above). The power of the GLGM2 model is reduced too much beyond degree 20 due to deweighting of the data. The uncertainty or RMS sigma of LP75G is too small due to the initial tight constraints on the gravity coefficients but was corrected for models that followed (LP100J, etc.). The observed power for all the *LP* models is about $2.5 \times 10^{-4}/n^2$. The farside gap causes a large uncertainty in the power spectrum beyond about degree 16–20. At this degree, the unconstrained solution strongly deviates from the power law and so becomes the limit for accurate global interpretation of the gravity field. Unfortunately, the investigation, for example, of a possible farside and nearside crustal dichotomy is limited to this degree. We also do not expect the actual power spectrum to be much larger than $2.5 \times 10^{-4}/n^2$ since the theoretical uncompensated gravity from topography from Smith *et al.* (1997) is near $3.5 \times 10^{-4}/n^2$.

Figure 6 shows the spectrum for the LP100J and LP165P models. The LP100K spectrum is very similar to LP100J. The aliasing in the last five degrees of the spectrum is evident for the LP100J model as it was for LP75G. The aliasing is much stronger for the lunar gravity models than what has been observed for

the Venus or Mars gravity models and is most likely due to the farside data gap together with low-altitude nonobserved farside spacecraft orbits. However, the aliasing was smoothed for the LP165P model at degrees 122, 145, and 165 as can be noted in the RMS sigma spectrum where an additional power constraint (2.0 to $5.0 \times 10^{-4}/n^2$ for each coefficient) was applied for only those 5 to 10 degree intervals to smooth the RMS spectrum. The determination of LP165P in three groups of coefficients as mentioned above has resulted in a RMS spectrum that is not as smooth as it would be if all the coefficients were estimated with one step. The spectrum is very smooth to degree 110 with very little noise but beyond this degree the noise increases although the resolution of many smaller features (such as Tycho crater) improves. Future efforts will be to develop a model that provides a smoother spectrum and less noisy result. With the noisier extended mission data, degree 165 seems to be about the limit of the data accuracy.

The second-degree coefficients of the lunar gravity field plus the lunar libration parameters (Dickey *et al.* 1994) give the normalized polar moment of inertia for the Moon (C/MR^2). The results for the LP100J, LP100K, and LP165P models are consistent with $C/MR^2 = 0.3932 \pm 0.0002$ and the lunar core constraints reported for the LP75G model (Konopliv *et al.* 1998). The solution for the polar moment is most sensitive to the relative data weight between the *LP* data and the *Clementine* data set (a 20% change in the relative data weight changes C/MR^2 by 0.0001). This sensitivity will remain until there is direct farside gravity observation at which time the uncertainty in the second-degree coefficients should significantly improve. Because of the farside gap, realistic uncertainties for the low-degree coefficients are perhaps as high as five times the formal uncertainties. The RMS differences between the coefficients of the LP100J and LP165P solutions are greater than the RMS uncertainties of LP100J by about a factor of 2 for coefficients less than degree 20. RMS

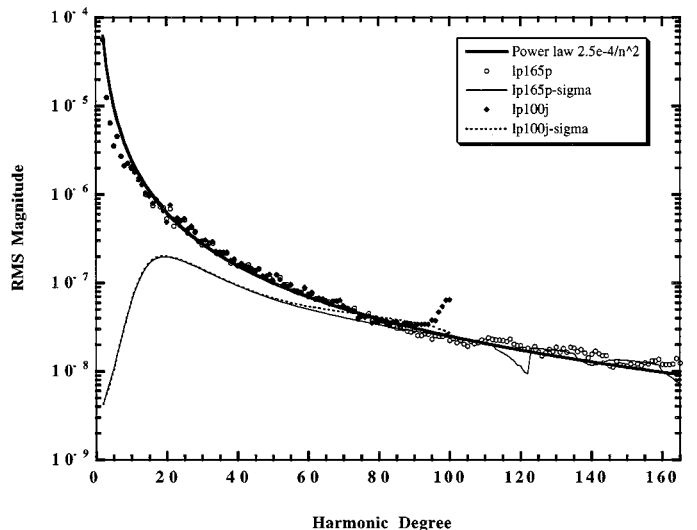


FIG. 6. RMS magnitude spectra for the higher degree and order lunar gravity solutions.

differences are significantly smaller than the uncertainties for coefficients with degree greater than 20.

The Love number solution for LP165P is $k_2 = 0.026 \pm 0.003$ (10 times the formal error) and it is even more sensitive to relative data weights and combinations than C/MR^2 . The k_2 information comes mostly from the time-varying solution for the C_{21} and S_{21} coefficients with the second largest contribution coming from the C_{22} and S_{22} variations. The zonal J_2 coefficient variations contribute little to the k_2 solution. Even with the large fluctuations in the k_2 solutions, results overall from various solutions tend to be less than the lunar laser ranging (LLR) result of $k_2 = 0.030 \pm 0.001$ (Dickey *et al.* 1994). The higher LLR result could be brought into agreement with the *LP* result by adding core ellipticity models to the LLR data (Dickey *et al.* 1994). Farside data would significantly reduce aliasing in the Love number solution and substantially improve the accuracy.

The maximum global resolution for the lunar topography is still the 90th degree solution from the *Clementine* laser altimeter (Smith *et al.* 1997) with a gap in the polar regions from 75° latitude and higher. Additional regions have been mapped in detail such as the polar nearside regions by Earth radio interferometry (Margot *et al.* 1999) and the full polar regions by *Clementine* stereo digital elevation maps (Cook *et al.* 2000), but as of yet no global high-resolution model has been pieced together. *LP* radio occultations (Asmar *et al.* 1999) give topographic height measurements along the lunar limb and may help resolve the absolute elevation differences of the radio interferometric and *Clementine* stereo models as pointed out by Cook *et al.* (2000). Once there is a higher resolution global model, evaluation of the high-resolution gravity will become easier. Figure 7 shows the correlation of the latest *LP* models (LP75G, LP100J, LP165P) with harmonic topography GLTM2 of Smith *et al.* (1997). Each subsequent model has shown an increase in correlation. The large negative correlation at degree 10 and continuing to about degree 20 is due to the lunar mas-

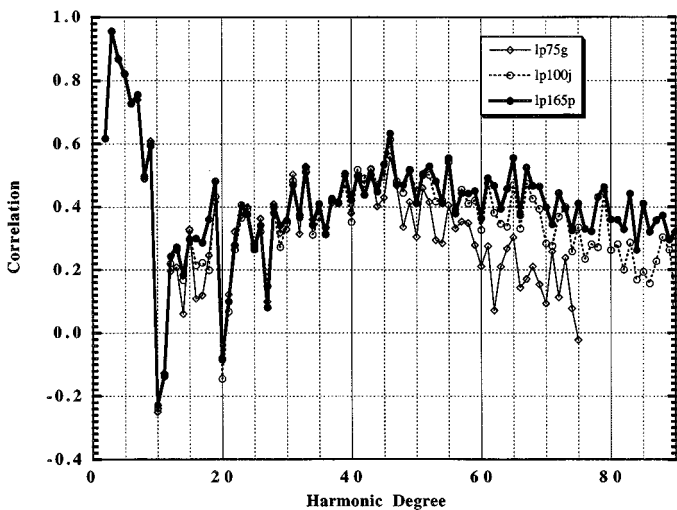


FIG. 7. Lunar gravity correlations with topography.

cons (mostly the five principal nearside mascons, Konopliv *et al.* (1998)).

The map of the gravity field LP165P at the lunar surface, as mentioned above, is very clean to degree 110 for the nearside. At degree 165 noise is visible in the solution, but geophysical interpretation to this degree may still be possible, but for purposes of display, Fig. 8 shows the vertical gravity at the lunar reference sphere with radius 1738.0 km without the J_2 coefficient for the nearside to degree 110 and for the farside to degree 60. Again displaying the farside to only degree 60 diminishes the noise in the map and more clearly shows the partial resolution of the farside features. There will always be a large amount of high-frequency noise for the farside until direct observation of the gravity is made. Since the geoid attenuates the high frequency, Fig. 9 shows both the farside and nearside potential surface to degree 110, again without the J_2 term. Contour lines are shown on these two plots for every 100 milligals for the vertical gravity and every 100 m for the geoid (solid black for positive and dashed white for zero or negative). Prominent on the nearside geoid are the mascons Imbrium and Serenitatis with magnitudes greater than 400 m. The farside highlands above and around Korolev and the large impact basin South-Pole Aitken are clearly visible on the lunar farside geoid with very little noise. Although much more detail is evident in the geoid for South-Pole Aitken, the long wavelength overall amplitude is similar to previous models such as GLGM2 (Lemoine *et al.* 1997). So conclusions of a mostly compensated basin from using the GLGM2 model remain unchanged (Zuber *et al.* 1994, Arkani-Hamed 1998).

Figures 10 and 11 show the corresponding uncertainties in the surface gravity and geoid from the full covariance matrix for the first 110 degrees of the LP165P solution (to match the highest degree with minimal noise). These formal errors are probably too optimistic and should be scaled upward by about a factor of 2. So nearside uncertainties are about 30 milligals or 4 m and farside uncertainties can be as large as 200 milligals or 60 m. The farside bifurcation of the errors (where there are larger uncertainties in the higher latitudes) is due to the multiple spacecraft (*LO* and *Apollo*) with inclinations between 0° and 30° . The crosshatched groundtracks provide various integrated observations of the farside gravity and somewhat reduce the farside uncertainties for those latitudes.

The most prominent features of the lunar gravity field are the mascons and are the result of a combination of a mantle plug and mare fill in the basin (see review in Konopliv *et al.* (1998)). Clearly visible on the nearside in both the acceleration and geoid are the five principal mascons Imbrium, Serenitatis, Crisium, Nectaris, and Humorum (clockwise from the upper left) that have been known since the *LO* missions. All features are mare-filled large impact basins. Each mascon anomaly has a significant contribution from the higher density mare relative to the crust (~ 3.3 vs ~ 2.9 gm/cm 3) as shown for Serenitatis by Phillips *et al.* (1972). All five of these mascons have sharp shoulders with a gravity plateau and a negative surrounding gravity anomaly. The newer *LP* gravity solutions, in general, improve the resolution

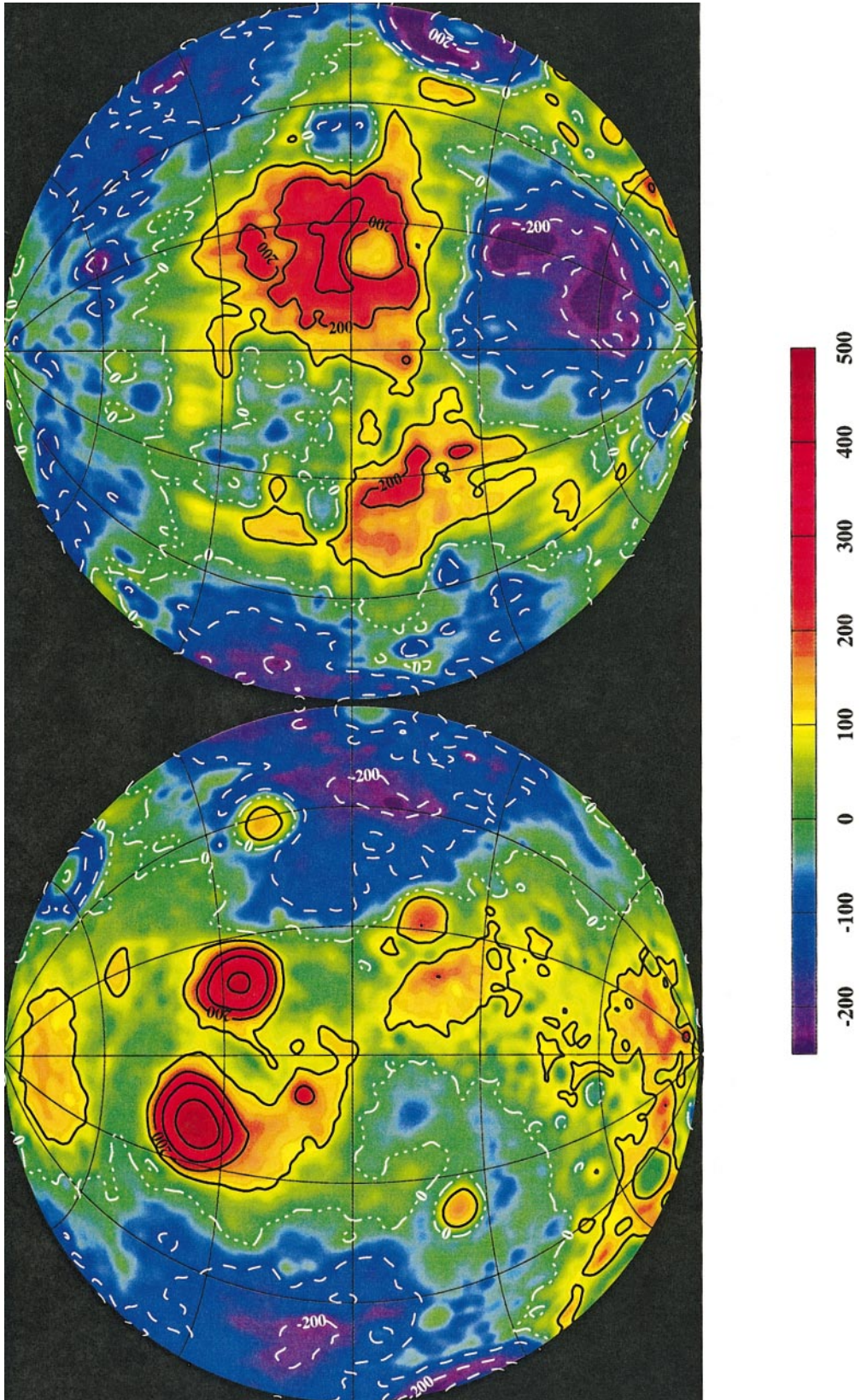


FIG. 9. Lunar geoid in meters with respect to the 1738-km reference sphere. Both the nearside (left) and farside (right) are evaluated to degree 110 of the LPI65F model.

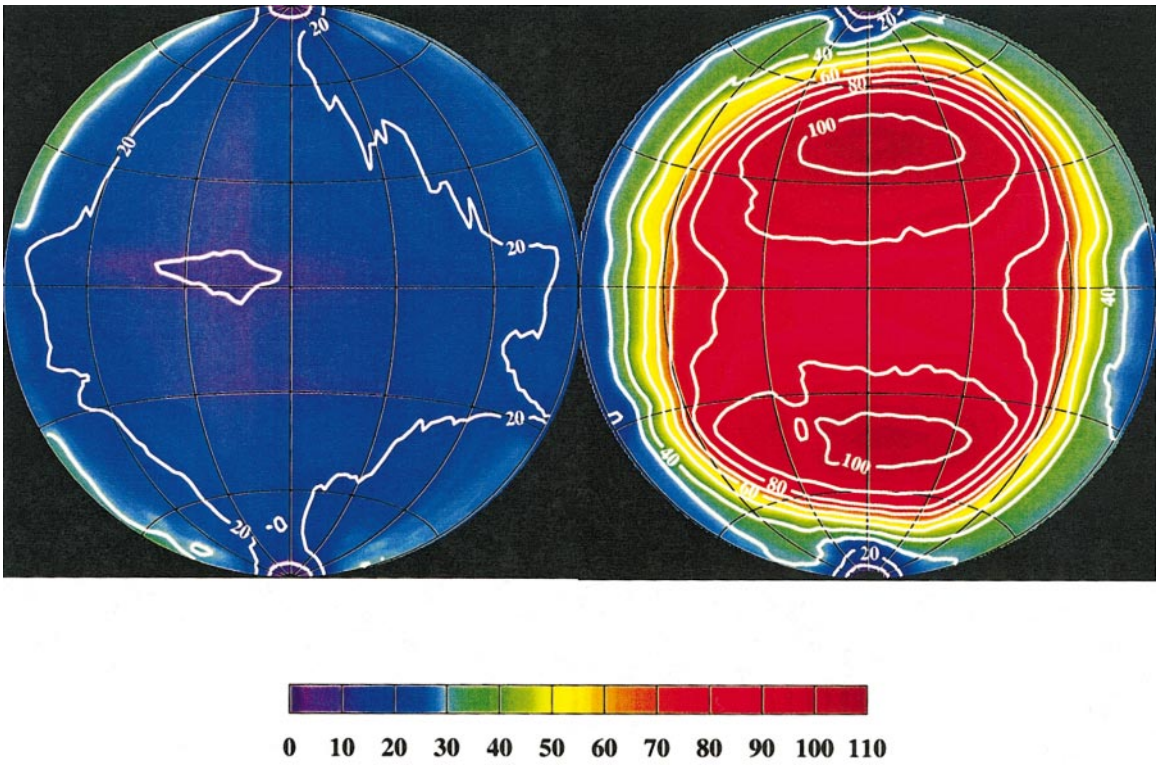


FIG. 10. Vertical gravity uncertainty at the lunar surface in milligals. The errors are from the full 110 degree covariance of the LP165P solution for both the nearside (left) and farside (right).

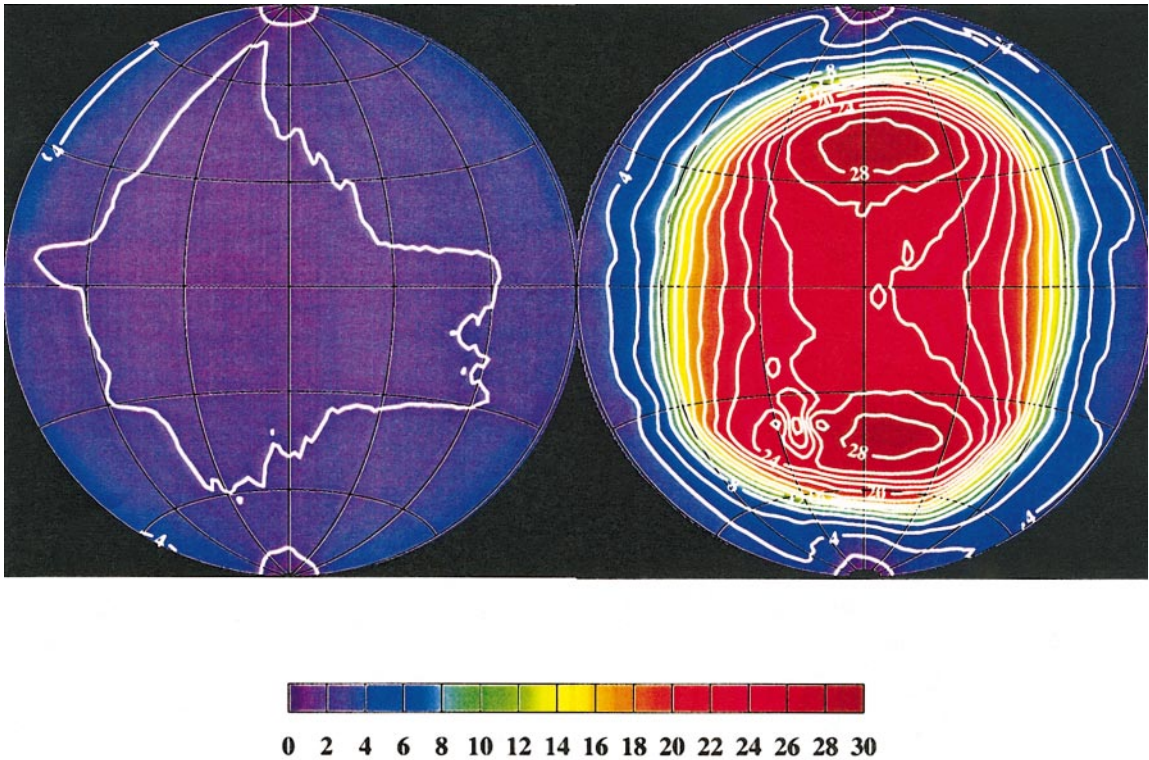


FIG. 11. Lunar geoid uncertainty at the lunar surface in meters. The errors are from the full 110 degree covariance of the LP165P solution for both the nearside (left) and farside (right).

of these mascons. It is now evident that Serenitatis has a double plateau. Just north of the main circular anomaly of 300-plus milligals is a very distinct shoulder with a smaller plateau of about 100 mgals that may be the result of mare fill in a depression (see Fig. 8).

The *LP* tracking data have clearly revealed many new additional mascons (currently 18) as listed in Table II. Gravity anomalies for the mascons are for LP165P to degree 110 (except for Schickard, which shows better resolution at degree 145). Amplitudes to degree 145 are generally nearly the same but significantly noisier and changes to degree 165 are not significant. For the new mascons, peak values are roughly the central max-

imum relative to the average surrounding negative ring within the basin. Absolute values are given for the previously known mascons from *LO* and *Apollo*.

Clearly evident are 12 new mascons for impact basins that are on the nearside or are close to the limb and so can be observed directly. For each mascon there are a circular negative anomaly in the outer parts of the basin relative to outside the crater limb and a central gravity high in the center of the basin relative to the negative ring. As an example, Fig. 12 shows the gravity contour lines for the Clavius mascon with an average basin ring minimum of -290 mgals and a central gravity peak of -170 mgals. Not included in the Table II list are other impact basins that

TABLE II
Lunar Mascons

Name	Absolute peak (mgals at $n = 110$)	Lat–Lon	Diameter ^a (km)	Age ^a
Previously Known Nearside Equatorial Mascons				
Imbrium	353	33°N, 18°W	1160	Lower Imbrium
Serenitatis	366	27°N, 19°E	740	Nectarian
Crisium	340	17.5°N, 58.5°E	1060	Nectarian
Humorum	325	24°S, 39.5°W	820	Nectarian
Nectaris	289	16°S, 34°E	860	Nectarian
Smythii	247	2°S, 87°E	840	Pre-Nectarian
Oriente	228	20°S, 95°W	930	Lower Imbrium
Grimaldi	261	5°S, 68°W	430	Pre-Nectarian
Lamont	166	6°N, 23°E	—	—
Cruger	192	17°S, 67°W	—	—
Aestuum	287	10°N, 10°W	—	—
Name	Relative peak (mgals at $n = 110$)	Lat–Lon	Diameter (km)	Age
New Nearside or Limb Mascons				
Humboltianum	380	61°N, 84°E	700	Nectarian
Mendel–Rydberg	360	50°S, 94°W	630	Nectarian
Schiller–Zucchi	350	56°S, 44.5°W	325	Pre-Nectarian
Amundsen–Ganswindt	360	81°S, 120°E	355	Pre-Nectarian
Schrodinger	260	75°S, 134°E	320	Lower Imbrium
Lorentz	260	34°N, 97°W	360	Pre-Nectarian
Harkhebi	190	40°N, 98°E	300	Pre-Nectarian
Deslandres	180	33°S, 5°W	234	Pre-Nectarian
Shickard	130 ^b	44°S, 55°W	227	Pre-Nectarian
Bailly	140	67°S, 68°W	300	Nectarian
Sikorsky–Rittenhouse	140	68°S, 110°E	270 ^c	Nectarian
Clavius	120	58°S, 14°W	225	Nectarian
Name	Relative peak (mgals at $n = 60$)	Lat–Lon	Diameter (km)	Age
Partially Resolved Farside Mascons				
Hertzprung	140	1.5°N, 128.5°W	570	Nectarian
Moscoviense	200	26°N, 147°E	445	Nectarian
Korolev	80	4.5°S, 157°W	440	Nectarian
Freundlich–Sharano	200	18.5°N, 175°E	600	Pre-Nectarian
Coulomb–Sarton	120	52°N, 123°W	530	Pre-Nectarian
Dirichlet–Jackson	160	14°N, 158°W	470	Pre-Nectarian ^c

^a Basin sizes and ages are from Wilhelms (1987) when available.

^b Peak at $n = 145$, peak is 70 mgals at $n = 110$.

^c Cook *et al.* (2000).

TABLE III
Gravity of Lunar Craters

Crater	Latitude	Longitude	Diameter (km)	Gravity floor (mgals)	Gravity rim (mgals)
Pre-Nectarian					
Balmer	-20	71	130	-100	-10
Barocius	-43	14	135	-365	+30
Blackett	-38	243	150	-266	+60
Boussinqualt	-71	55	120	-451	0
Brianchon	+74	271	120	-415	-40
Curie	-23	92	139	-280	0
Eddington	+22	288	120	-122	-20
Einstein	+17	271	170	-146	0
Furnerius	-36	60	125	-255	+20
Goldschmidt	+73	357	120	-125	0
Gruemberger	-64	338	100	-324	0
Hecataeus	-21	80	120	-410	0
Helmholtz	-69	65	110	-301	-10
Herschel	+62	319	120	-158	0
Hipparchus	-6	5	151	-50	+40
Hirayama	-6	94	139	-333	-100
Janssen	-46	41	200	-234	+50
Joliet	+26	93	150	-284	-40
Landau	+43	241	221	-334	0
Lippmann	-56	244	130	-373	0
Lytot	-50	84	141	-203	0
Maginus	-50	354	163	-375	+50
Manzinus	-68	25	110	-268	-20
Maurolucus	-42	14	150	-365	+30
Mee	-43	325	100	-271	-50
Messala	+39	60	124	-94	0
Milne	-31	113	262	-230	0
Moretus	-71	355	120	-380	0
Pasteur	-11	105	235	-261	+100
Piazzi	-37	292	120	-207	0
Poczobutt	+57	260	200	-290	-40
Ptolemaeus	-9	358	153	-100	+10
Purbach	-26	358	118	-75	+60
Rosenberger	-55	43	96	-186	-70
Rozhdestvenskiy	+85	208	150	-451	-120
Sacrobosco	-55	17	98	-120	+60
Scheiner	-61	331	120	-270	+20
Schickard	-44	305	227	-228	-20
Schiller	-52	320	160	-284	0
Skłodowska	-17	97	120	-310	0
Stofler	-41	6	126	-198	+50
Szilard	+34	106	127	-196	0
Vendelinus	-16	61	100	-219	-50
Werner	-28	3	100	-66	+50
Xenophanes	+58	278	120	-233	-80
Nectarian					
Albategnius	-11	4	136	-264	+30
Alphonsus	-15	358	119	-144	-10
Cleomedes	+28	56	126	-314	-20
Demonax	-78	60	100	-409	0
Endymion	+54	57	125	-281	0
Gauss	+36	79	177	-144	0
Hevelius	+2	293	106	-121	0
Hilbert	-18	108	170	-348	+40
Huggins	-40	356	120	-236	-60
Longomontanus	-50	338	145	-405	0
Neper	+9	85	137	-337	+20

TABLE III—Continued

Crater	Latitude	Longitude	Diameter (km)	Gravity floor (mgals)	Gravity rim (mgals)
Oken	-44	76	110	-148	-70
Pascal	+74	290	100	-258	0
Phecolides	-53	302	130	-193	0
Pitatus	-30	346	97	-96	0
Schwarzchild	+71	120	235	-400	-60
Vieta	-29	304	105	-230	+30
Zeeman	-75	225	160	-489	-40
Lower Imbrian					
Arzachel	-18	358	97	-206	0
Compton	+56	105	162	-314	0
Petavius	-25	60	177	-182	-20
Upper Imbrian					
Humboldt	-27	81	207	-200	0
Iridum	+44	329	260	-231	-80
Piccolomini	-30	32	88	-101	0
Eratosthenian					
Aristoteles	+50	17	87	-165	-20
Hausen	-66	272	167	-397	0
Langrenus	-9	61	132	-461	-60
Pythagoras	+64	297	130	-381	-40
Theophilus	-11	26	100	-203	+120
Copernican					
Copernicus	+10	340	93	-180	+40
Tycho	-43	249	85	-134	0

Note. Crater location, size, and age are given by Wilhelms (1987) in Tables 8.3, 9.4, 10.2, 11.2, 12.2, 13.1. Ages of craters not listed in these tables are determined as best as possible from Plates 6–11. The gravity amplitudes are from LP165P truncated at degree 110 and include the J_2 term.

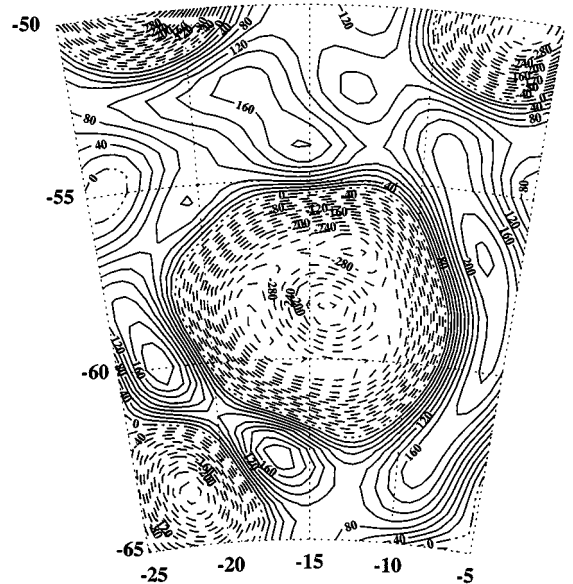


FIG. 12. Vertical gravity for the Clavius crater showing the gravity peak in the center of the crater. The gravity is from a 110 degree truncation of the LP165P model with the J_2 term removed. The contour lines are in 20-milligal intervals.

do not show a central gravity peak in the center of the basin; for example, Tranquillitatis, Nubium, and Australe have a mixture of gravity highs and lows but no clear circular feature is evident with a gravity high in the center. Fecunditatis is closer in that it has a minor central gravity high but the circular features are not clearly evident. Other smaller impact basins such as Pasteur, Milne, and Schwarschild show a circular negative gravity corresponding to the basin but do not currently have a clear central peak. They may be later classified as mascons as the resolution of the lunar gravity model improves. Even so, craters as small as 225 km (Shickard, Clavius) show a large central gravity high within the basin. Also not included in the mascon list are several small circular positive gravity features that correspond to topographic lows such as two in Tranquillitatis (13°N, 30°E at 200 mgals and 17°N, 35°E at 180 mgals) and one near Smythii (0°N, 79°E at 240 mgals) that may be from buried impact basins with mantle plugs or are mare-filled craters. Vaporum with a gravity amplitude of 87 mgals that is close to the second plateau value of Serenitatis is most likely just mare fill. All the new mascons (except Humboldtianum and partly Mendel-Rydberg) have no evidence of mare fill and so are most likely a result of a denser mantle plug.

Since the lunar farside gravity is not directly observed, it is difficult to identify mascons on the farside. However, we believe there are strong indications of mascons for six large farside basins as listed in Table II. Most of these features have been identified before as negative anomalies (Ananda 1977, Konopliv *et al.* 1993, Lemoine *et al.* 1997). However, in the *LP* models it has become apparent that these features also have a central gravity high in the center of the basin with a surrounding negative ring. In fact, the appearance of a mascon north of Korolev led to the confirmation of the Dirichlet–Jackson basin by the *Clementine* stereo elevation data (Cook *et al.* 2000). The mascons are only partially resolved and require information from all the previous missions (*LO*, *Apollo*) to be seen. The corresponding gravity highs around the basins do not match as well with the topographic highs as does the nearside gravity, and the amplitude of the central peak is about one-third of the value of what one would expect based upon the nearside mascons. So it is not possible to determine mantle plug size and look for correlations with basin size or age. All that can be said is that they likely exist. Many other farside basins such as Ingenii, Planck, Birkhoff, Mendeleev, and Poincare will probably turn out to be mascons once the farside gravity is directly observed since most nearside basins of corresponding age and size are mascons. The amplitudes in Table II are given through degree 60 using the LP165P model, although amplitudes can change somewhat for different models. The LP165P amplitudes are strong for Moscoviense and Freundlich–Sharanov but LP100J and LP100K show better peaks for the Hertzprung and Korolev basins.

In addition to the mascons, the *LP* gravity models resolve many craters to diameters near 100 km or larger. Table III gives a partial list of craters where they are listed by age group as described by Wilhelms (1987). Gravity values are given for the

floors and approximate rims, which for many craters are not very clear since rims are not complete and are cut off by other craters. The values were produced from the 165th degree and order model but were evaluated at 110th degree and order. Two examples of crater resolution are shown in Fig. 13 for Neper and Cleomedes. One can further refine most craters by additional analysis of the LOS Doppler residuals from the very low-altitude orbits obtained near the end of the *Lunar Prospector* mission, for there are significant signatures remaining after the extraction of the spherical harmonic model. Also, future higher degree single-step spherical harmonic models ($n > 110$) will improve crater

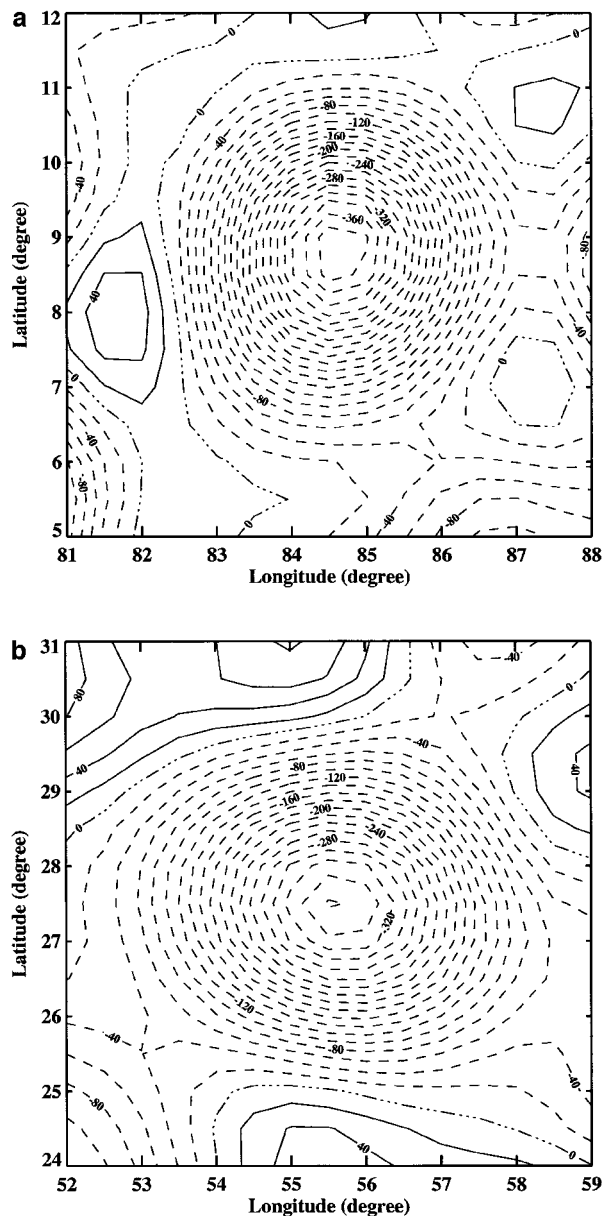


FIG. 13. Vertical gravity for the crater (a) Neper and (b) Cleomedes. The gravity is from a 110 degree truncation of the LP165P model with the J_2 term removed. The contour lines are in 20-milligal intervals.

resolution. Analysis of the degree of isostatic compensation for each crater versus age and location could possibly provide information on thermal history of the Moon.

Overall, the latest gravity field model LP165P is a significant improvement from previous models in providing a clean spectral solution to degree 110 (versus about degree 90 for LP100J or LP100K) and is the model of choice for geophysical interpretation. With LP165P, the *Lunar Prospector* mission has identified 18 new mascons, resolved numerous craters, and provided an initial dynamic Love number estimate ($k_2 = 0.026$). For orbit determination, LP100K is probably the model to use because of excessive compute times with LP165P. There is still room for improvement with the lunar gravity models even with the existing tracking data. A complete high-resolution solution (\sim degree 150) in one step (i.e., one complete information array) would be a significant improvement over LP165P. The limiting factor is the amount of computing time such a solution would take, but hopefully, computer resources will become available to pursue such a model. Also, a higher resolution global model of the topography is needed for evaluation of the gravity model as well as geophysical interpretation. This topography model is currently being developed using the *Clementine* stereo elevation data (see Cook *et al.* (2000) for polar results), and, of course, best of all would be direct farside measurement of the gravity field. The subsatellite tracking of the Japanese *SELENE* mission scheduled for launch in 2003 will fill the farside data gap and greatly improve the lunar gravity field. It will even make the existing *LP* data more valuable in, for example, investigating the Love number and improved polar moment.

ACKNOWLEDGMENTS

The HP SPP2000 Supercomputer used in this investigation was provided by funding from the NASA Offices of Mission to Planet Earth, Aeronautics, and Space Science. The research described in this paper was carried out by the Jet Propulsion Laboratory, California Institute of Technology, under a contract with the National Aeronautics and Space Administration.

REFERENCES

- Akim, E. L. 1966. Determination of the gravitational field of the Moon from the motion of the artificial lunar satellite "Lunar-10." *Dokl. Akad. Nauk SSSR* **170**, 799–802.
- Ananda, M. P. 1977. Lunar gravity: A mass point model. *J. Geophys. Res.* **82**, 3049–3064.
- Arkani-Hamed, J. 1998. The lunar mascons revisited. *J. Geophys. Res.* **103**, 3709–3739.
- Asmar, S., G. Schubert, A. Konopliv, and W. Moore 1999. Improving on the high latitude topography of the Moon via precise timing of the Lunar Prospector radio occultations. In *31st Annual Meeting of the Division of Planetary Sciences, 10–15 Oct. 1999, Padua, Italy*.
- Barriot, J. P., N. Valès, G. Balmino, and P. Rosenblatt 1998. A 180th degree and order model of the Venus gravity field from Magellan line-of-sight residual Doppler data. *Geophys. Res. Lett.* **25**, 3743–3746.
- Bierman, G. J. 1977. *Factorization Methods for Discrete Sequential Estimation*, Academic Press, New York.
- Bills, B. G., and A. J. Ferrari 1980. A harmonic analysis of lunar gravity. *J. Geophys. Res.* **85**, 1013–1025.
- Binder, A. B. 1998. Lunar Prospector: Overview. *Science* **281**, 1475–1476.
- Binder, A. B., W. C. Feldman, G. S. Hubbard, A. S. Konopliv, R. P. Lin, M. H. Acuna, and L. L. Hood 1998. Lunar Prospector searches for polar ice, a metallic core, gas release events, and the Moon's origin. *EOS Trans.* **79**, 97.
- Carranza, E., A. Konopliv, and M. Ryne 1999. Lunar Prospector orbit determination uncertainties using the high resolution lunar gravity models. In *AAS/AIAA Astrodynamics Specialist Conference, Girdwood, AK, August*, AAS Paper 99-325.
- Cook, A. C., T. R. Watters, M. S. Robinson, and P. D. Spudis 2000. Lunar polar topography derived from Clementine stereo images. *J. Geophys. Res.* **105**, 12,023–12,033.
- Davies, M. E., V. K. Abalakin, A. Brahic, M. Bursa, B. H. Chovitz, J. H. Lieske, P. K. Seidelmann, A. T. Sinclair, and Y. S. Tjuffin 1992. Report of the IAU/IAG/COSPAR Working Group on cartographic coordinates and rotational elements of the planets and satellites: 1991. *Celest. Mech.* **53**, 377–397.
- Davies, M. E., V. K. Abalakin, M. Bursa, J. H. Lieske, B. Morando, D. Morrison, P. K. Seidelmann, A. T. Sinclair, B. Yallop, and Y. S. Tjuffin 1996. Report of the IAU/IAG/COSPAR Working Group on cartographic coordinates and rotational elements of the planets and satellites: 1994. *Celest. Mech. Dynam. Astron.* **63**, 127–148.
- Dickey, J. O., P. L. Bender, J. E. Faller, X. X. Newhall, R. L. Ricklefs, J. G. Ries, P. J. Shelus, C. Veillet, A. L. Whipple, J. R. Wiatt, J. G. Williams, and C. F. Yoder 1994. Lunar laser ranging: A continuing legacy of the Apollo program. *Science* **265**, 482–490.
- Ellis, J. 1980. Large scale state estimation algorithms for DSN tracking station location determination. *J. Astronaut. Sci.* **28**, 15–30.
- Ferrari, A. J. 1977. Lunar gravity: A harmonic analysis. *J. Geophys. Res.* **82**, 3065–3084.
- Ferrari, A. J., W. S. Sinclair, W. L. Sjogren, J. G. Williams, and C. F. Yoder 1980. Geophysical parameters of the Earth–Moon system. *J. Geophys. Res.* **85**, 3939–3951.
- Kaula, W. M. 1966. *Theory of Satellite Geodesy*. Blaisdell, Waltham, MA.
- Konopliv, A. S., and W. L. Sjogren 1995. The JPL Mars gravity field, Mars 50c, based upon Viking and Mariner 9 Doppler tracking data. Tech Report, Jet Propulsion Laboratory, California Institute of Technology, Pasadena, CA.
- Konopliv, A. S., and C. F. Yoder 1996. Venusian k_2 tidal Love number from Magellan and PVO tracking data. *Geophys. Res. Lett.* **23**, 1857–1860.
- Konopliv, A. S., and D. N. Yuan 1999. Lunar Prospector 100th degree gravity model development. *Lunar Planet. Sci. Conf. 30th*, Abstract 1067. Lunar and Planetary Institutes, Houston.
- Konopliv, A. S., W. B. Banerdt, and W. L. Sjogren 1999. Venus gravity: 180th degree and order model. *Icarus* **139**, 3–18.
- Konopliv, A. S., A. B. Binder, L. L. Hood, A. B. Kucinskis, and J. G. Williams 1998. Improved gravity field of the Moon from Lunar Prospector. *Science* **281**, 1476–1480.
- Konopliv, A. S., W. L. Sjogren, R. N. Wimberly, R. A. Cook, and A. Vijayaraghavan 1993. A high resolution lunar gravity field and predicted orbit behavior. In *AAS/AIAA Astrodynamics Specialist Conference, Victoria, B.C., Canada, August*, AAS Paper 93-622.
- Lawson, C. L., and R. J. Hanson 1995. *Solving Least Squares Problems*, SIAM Classics in Applied Mathematics, Vol. 15. Society for Industrial and Applied Mathematics, Philadelphia.
- Lemoine, F. G., D. E. Smith, M. T. Zuber, G. A. Neumann, and D. D. Rowlands 1997. A 70th degree lunar gravity model (GLGM-2) from Clementine and other tracking data. *J. Geophys. Res.* **102**, 16,339–16,359.
- Liu, A. S., and P. S. Laing 1971. Lunar gravity analysis from long term effects. *Science* **173**, 1017–1020.
- Lorell, J., and W. L. Sjogren 1968. Lunar gravity: Preliminary estimates from lunar orbiter. *Science* **159**, 625–628.

- Margot, J. L., D. B. Campbell, R. F. Jurgens, and M. A. Slade 1999. Topography of the lunar poles from radar interferometry: A survey of cold trap locations. *Science* **284**, 1658–1660.
- McKenzie, D., and F. Nimmo 1997. Elastic thickness estimates for Venus from line of sight accelerations. *Icarus* **130**, 198–216.
- Michael, W. H., Jr., and W. T. Blackshear 1972. Recent results on the mass, gravitational field and moments of inertia of the Moon. *Moon* **3**, 388–402.
- Moyer, T. D. 1971. Mathematical formulation of the double-precision orbit determination program (DPODP). JPL Technical Report 32-1527, Jet Propulsion Laboratory, California Institute of Technology, Pasadena, CA.
- Muller, P. M., and W. L. Sjogren 1968. Mascons: Lunar mass concentrations. *Science* **161**, 680–684.
- Neumann, G. A., M. T. Zuber, D. E. Smith, and F. G. Lemoine 1996. The lunar crust: Global structure and signature of major basins. *J. Geophys. Res.* **101**, 16,841–16,863.
- Newhall, XX and J. G. Williams 1997. Estimation of the lunar physical librations. *Celest. Mech. Dynam. Astron.* **66**, 21–30.
- Phillips, R. J., J. E. Conel, E. A. Abbott, W. L. Sjogren, and J. B. Morton 1972. Mascons: Progress toward a unique solution for mass distribution. *J. Geophys. Res.* **77**, 7106–7114.
- Smith, D. E., W. L. Sjogren, G. L. Tyler, G. Balmino, F. G. Lemoine, and A. S. Konopliv 1999. The gravity field of Mars: Results from Mars Global Surveyor. *Science* **286**, 94–97.
- Smith, D. E., M. T. Zuber, G. A. Neumann, and F. G. Lemoine 1997. Topography of the Moon from the Clementine lidar. *J. Geophys. Res.* **102**, 1591–1611.
- Wilhelms, D. E. 1987. The geologic history of the Moon. U.S. Geol. Surv. Prof. Pap. 1348, U.S. Government Printing Office, Washington, DC.
- Williams, J. G., XX Newhall, and J. O. Dickey 1996. Lunar moments, tides, orientation, and coordinate frames. *Planet. Space Sci.* **44**, 1077–1080.
- Wong, L., G. Buechler, W. Downs, W. Sjogren, P. Muller, and P. Gottlieb 1971. A surface-layer representation of the lunar gravity field. *J. Geophys. Res.* **76**, 6220–6236.
- Yuan, D. N., W. L. Sjogren, A. S. Konopliv, and A. B. Kucinskas 2000. The gravity field of Mars: A 75th degree and order model. *J. Geophys. Res.*, submitted.
- Zuber, M. T., D. E. Smith, F. G. Lemoine, and G. A. Neumann 1994. The shape and internal structure of the Moon from the Clementine mission. *Science* **266**, 1839–1843.